Molecular BioSystems

Accepted Manuscript

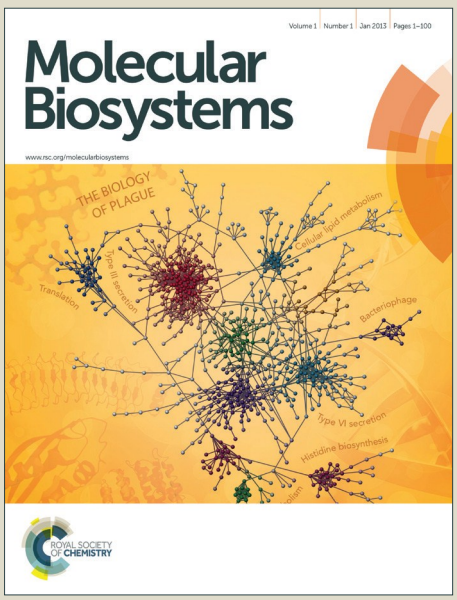

ROYAL SOCIETY OF CHEMISTRY

www.rsc.org/molecularbiosystems

Detailed Computational Analyzes Revealed Mutation V210I on PrP Induced Conformational Conversion on β2-α2 loop and α2-α3

P. Chandrasekaran and R. Rajasekaran*

Computational biology lab, Department of Biotechnology, School of Biosciences and Technology, VIT University, Vellore 632 014, Tamil Nadu, India

Abstract

The development of fatal transmissible spongiform encephalopathies (TSE) is associated with the conformational conversion of the normal cellular prion protein, PrP^{C} into its pathogenic isoform, PrP^{Sc}. The present study revealed the structural consequences which induce the conversion of $PrP^{C}\rightarrow PrP^{Sc}$ upon mutation V210I linked with genetic Creutzfeldt-Jakob disease (CJD) using classical molecular dynamics (MD) approach. Similar to the experimental results, mutant showed biased disruption in the local folding of α2 and the complete distortion on α3. In addition, substitution of bulkier Ile at position 210 induced reorientations of several residues that were the constituent of hydrophobic core, thereby influencing α2-α3 inter-helical interactions. In addition, the β2-α2 loop was altered greatly, due to the loss of π-π interactions of residue Tyr^{169} with Phe^{175}, Tye^{163}, Tyr^{162}, and Tyr^{218}, facilitating more conformational flexibility which may involved in the conversion of $PrP^{C}\rightarrow PrP^{Sc}$. This study afforded a detailed structure and dynamic properties of mutant which were consistent with experimental results, providing insight into the molecular basis for the conversion of $PrP^{C}\rightarrow PrP^{Sc}$ could be used for the development of antiprion drugs.

Key words: Prion protein, mutation V210I, β2-α2 loop, molecular dynamics.

Introduction

Aggregation of misfolding protein is often associated with various diseases in human such as Alzheimer's disease, Parkinson's disease, type II diabetes, and other several forms systemic amyloidosis.[1,2] The present work emphasizes one of the well-known and the aggregation forming propensity of Prion protein (PrP). PrP is an endogenous and evolutionarily conserved membrane-bound protein present in neuronal cells of mammals.[3] Mutations in PRNP gene are associated with prion diseases. Prion diseases or transmissible spongiform encephalopathies (TSE) are a group of neurodegenerative diseases such as scrapie in sheep, bovine spongiform encephalopathy (BSE) in cattle, and Creutzfeldt-Jakob disease (CJD), Gerstmann-Straussler-Scheinker disease, fatal familial insomnia, and kuru in humans, which are sporadic, inherited, or acquired.[4-7] These diseases are attributed to the conversion of the normal cellular prion protein (PrP^{C}) to its misfolded pathogenic form PrP^{Sc}.[5,8,9] PrP is a 209 residues glycoprotein, contains N-terminal unstructured region and the C-terminal globular, folded domain. The N-terminal region (residues: 23-120) is consists of highly disordered and can to bind Cu^{2+} ions. The C-terminal domain (residues: 126-231) is mostly comprised of an ordered three α-helices (helix α1, 144-154; helix α2, 173-195; helix α3, 200-226) and two short anti-parallel β-strands (127-130 and 162-165).[10-13] In particular, the α2-α3 regions are mainly Involved in the conformational transition of $PrP^{C} \rightarrow PrP^{Sc}$.[14-16] PrP^{C} is monomeric, soluble, and protease-sensitive, whereas PrP^{Sc} is highly insoluble and protease-resistant.[7,17] Thus, notable differences in the physio-chemical properties between PrP^{C} and PrP^{Sc} is arising from their conformation.[18] Because, the content of α-helices decreases to some extent during the conformational transition of PrP^{C} to PrP^{Sc}, but the content of β-sheet increases greatly.[6] Nevertheless, the complete structure of PrP^{Sc} is still not un-known; several study states that conformational conversion of PrP^{C} to PrP^{Sc} entails, at least, partial refolding of the C-terminal domain.[19] Therefore, characterization of the conformational dynamics adopted by PrP upon various mutations is a challenging task in the field of structural biology.

To better understand the structural disorder caused by the pathological mutation V210I at the atomistic level, we have performed molecular the dynamics (MD) simulation for the wild-type (WT) PrP and its mutant V210I. This hydrophobic mutation was responsible for the development of familial CJD, and it was identified as common mutation noticed among genetic

TSE cases in the European population.[20] MD results revealed that mutant V210I exhibited some structural features that were not present in WT-PrP. These structural findings provided some valuable information about the possible key determinants underlying the molecular mechanism of prion conversion, correlated well with the experimental studies.[19,20]

Materials and methods

MD simulation set up

The atomic coordinates contained in the 1QM1 and 2LEJ files were used to set up the simulation of WT-PrP (number of atoms: 1694) and its mutant V210I (number of atoms: 1697) respectively. MD simulations were performed by Gromacs 4.5.5 package.[21,22] Both the WT-PrP and its mutant were parameterized with OPLS force field.[23] After, both the WT-PrP and its mutant have been immersed in cubic boxes separately and filled with simple point-charge (SPC) water molecules, imposing a minimal distance between the solute and the box walls of 1.2 nm. Three counter ions, Na^+ were added as required to neutralize the total charge of both the WT-PrP and its mutant system using the Genion utility of Gromacs. The solvated structures were energy minimized using the steepest descent method and the Particle Mesh Ewald (PME)[24] method was used to treat long-range electrostatic interactions. The van der Waals and Coulomb cut-off were used as 14 Å and 10 Å respectively. The SHAKE algorithm[25] was used to constrain the bond lengths involving in hydrogen atoms. The canonical ensemble (NVT) was carried out for 100 ps, during which the systems were heated from 100 to 300 K after the required energy minimization process. Subsequently, isothermal-isobaric ensemble (NPT) MD was performed for 100 ps to adjust the solvent density using V-rescale and Berendsen's weak coupling algotithm.[26] The production runs of all MD simulations achieved the lengths of 50 ns, and the coordinates were saved at regular time intervals of every 2 ps. The solvent-accessible surface area of residues from α-helices in the WT-PrP and its mutant were predicted by using WHAT IF program.[27]

Order parameter

To quantify the flexibility of amino-acid side chains, we used dihedral order parameters for torsion angles from side chains (χ-angles), as described in vander Spoel and Berendsen.[28] Briefly, from using the probability distribution $p(\theta)$ of a given dihedral angle θ, the

autocorrelation function C(∞) of this dihedral angle at infinite times is calculating

$$C(\infty) = \left(\int_0^{2\pi} \cos(\theta)\, p\,(\theta) d\theta\right)^2 + \left(\int_0^{2\pi} \sin(\theta)\, p\,(\theta) d\theta\right)^2$$

yielding an order parameter S2D=C(∞)[29] between zero (full flexibility) and one (no flexibility). For each residue, the lowest calculated order parameter was used. Calculations were performed using the Gromacs utility g_chi.[30]

Principal component analysis

Principal component analysis (PCA) is a method commonly used for dissecting functional significance of the correlated motion of protein and their importance in biological processes, such as substrate binding or protein folding. We applied g_covar utility of Gromacs to obtain the C_α covariance matrix for both the WT-PrP and its mutant from 50 ns of the trajectories. Rotational and translational motions were removed before covariance matrix calculation by least-squares superposition to the averaged-structure. The covariance matrix, C for each element is represented by:

$$Cij = \langle (xi - \langle xi \rangle)(xj - \langle xj \rangle) \rangle$$

where xi and xj are the internal coordinates of atoms, i and j and all analyzes were performed with the g_anaeig module of Gromacs. A set of eigenvalues and eigenvectors were identified by diagonalizing the matrix. Each eigenvector thus represented a single correlated displacement of a group of atoms in a multidimensional space and the eigenvalues were the amplitude of the motion along the eigenvector. Eigenvectors were then sorted according to their eigenvalues in decreasing order. The eigenvectors associated with the highest eigenvalues described the principal components of motion. It had been shown that the first few eigenvectors could successfully describe almost all conformational sub-states accessible to the protein. Only a few eigenvectors were needed to explain a large part of the total variance, as the motions are highly correlated, i.e., collective.[1,31-33]

Results and discussion

Relationship between simulation and experiment

Before carrying out detailed analyzes, it is essential to ensure the reliability of simulation with experimental data produced by NMR: a method that has provided more structural information on PrP. To do this, we have calculated the chemical shift values from our simulations (δ_{sim}) and compared with those determined by experimentally (δ_{exp}). The chemical shift values of WT-PrP and its mutant V210I were calculated by the SHIFTX2[34] program based on the ensemble of conformation at 278 K and the pH of 7. Further, we have confirmed the association between the simulation and experimental chemical shift value as depicted in Fig. 1. It should be noted that a slight standard deviation was observed between the chemical shift value of simulation and the experiment, indicating the convergence of simulation by exhibiting the similar kind of chemical shift values as observed from the experimental result. The C_α chemical shift value of WT-PrP calculated from δ_{sim} was greatly correlated with those observed in δ_{exp} (r=0.95). Similarly, C_α chemical shift of mutant V210I calculated from δ_{sim} was significantly associated with δexp (r=0.89). Interestingly, C_β chemical shift value of WT-PrP and its mutant V210I calculated from δ_{sim} was highly correlated with those determined by δ_{exp} (r=0.99). In a nutshell, chemical shift value of MD simulation showed a great association with those determined by experimentally, indicating that simulation also reproduced the structural ensemble of NMR as well.

Transition of secondary structures revealed by DSSP

We have first investigated and compared the secondary structural profile of WT-PrP and its mutant. Transition of one secondary structure state into another was involved in the conversion of PrP^C into its pathogenic state, PrP^{Sc}. Therefore, knowledge about the secondary structure elements was needed to understand the influence of mutation V210I on PrP, for which DSSP analysis was performed.[35] The time evolution of secondary structure elements present in WT-PrP and its mutant as represented in Fig. 2. It was found that WT-PrP exhibited α1 residues: 144-154) positioned between β1-β2 and also displayed a 3_{10}-helix (residues: 155-158) at the end of α1, similar type observations also reported by the experimental study.16 In the WT-PrP, a firm and stable α2 (residues: 172-188) was examined, meanwhile, some of trajectories were also

displayed an elongated α2 during the simulation period. Furthermore, the WT-PrP established a long α3 (residues: 200-224) as noticed approximately up to 12 ns, thereafter α3 was disrupted by the development of turn segment (residues: 207-210), roughly around 45 ns simulation period. In contrast to WT-PrP, mutant displayed an elongated α1, by losing its 3_{10}-helix at the end of α1. In addition, mutant also lost another structurally important 3_{10}-helix (residues: 166-169) as positioned in the β2-α2 loop. Moreover, mutant displayed a major structural rearrangement in the N-terminal part of α2 and also at the C-terminal region of α3. This notable structural perturbation was totally influenced by the loss of M-M hydrogen bonds, mainly involved in the local folding of α-helices and beta-sheet, thereby mutant able to develop the turn, 3_{10}-helix and bend regions. Interestingly, this result was well correlated with the experimental report; it stated that the reduced number of long-range NOE contacts influenced more structural variations in the N-terminal region of α2 and also at the C-terminal part of α3.[19]

Further, we have extended our analysis in-depth manner by identifying the number of residues involved in the each state of secondary structure in the WT-PrP and its mutant. The time evolution of number of residues involved in the secondary structure profile of WT-PrP and its mutant as illustrated in Sup Fig. 1. It was found that the amount of residues involved in the coil, β-bridge, bend, turn, and 3_{10}-helix were increased significantly in mutant, particularly the amount of residues employed in turn, bend, and 3_{10}-helix region raised remarkably when compared to the WT-PrP. Conversely, the number of residues engaged in α-helices and β-sheets were decreased in the mutant; especially the numbers of residues that involved in α-helices were reduced greatly. In addition, comparison of secondary structure results showed that WT-PrP comprised of 47% α-helices, whereas mutant consisted of 31% α-helices, only a slight variation was observed in the content of β-sheet.

Rationale for distortion in the local folding of α2-α3

Interactions within a protein were essential consideration for understanding the stability and function of protein. There were numerous weak and strong interactions that render stability to a protein, among hydrogen bond plays a vital role in the folding of α-helices and β-sheets.[36,37] Thus, it's essential to correlate the relationship between hydrogen bonding interactions and folding of mutant. To accomplish this, we have calculated the intra-molecular hydrogen bonding

interactions in the WT-PrP (green) and its mutant V210I (indigo) as depicted in Fig. 3A. The numbers of hydrogen bonds were reduced greatly in mutant when compared to WT-PrP, indicating the structural instability. Further, to describe the observed disturbance in the local folding of α2-α3, it is essential to identify the number of hydrogen bonds were formed by backbone atoms. Accordingly, hydrogen bonds were classified into three types based on its atomic interactions: main chain-main chain (M-M), main chain-side chain (M-S), and side chain-side chain (S-S) hydrogen bonds. This result showed that mutant comprised of decreasing in M-M hydrogen bonds further which confirmed the disturbance in the local folding of α2-α3, remarkably reduced the numbers of residues involved in those helices. It has also been stated that the number of interactions was almost proportional to the number of residues involved in a protein.[38] Collectively, the regular secondary structural elements such as α-helix, 3_{10}-helix, and β-sheet in the WT-PrP comprised of a total of 14,036,89 residues and were involved in the formation of 11,023,28 M-M hydrogen bonds. On the other hand, mutant consisted of a total of 11,38,378 residues and established the number of hydrogen bonds as 88,5450, indicating the influence of mutation on its structure. The observed reduction in the content of α2-α3 in mutant due to the loss M-M hydrogen bonds mediated by i^{th} and $i+4^{th}$ residues. Likely, the amount of M-S (Fig. 3C) and S-S (Fig. 3D) hydrogen bonds were also reduced in mutant when compared to WT-PrP, suggesting the overall structural rearrangement of mutant.

Several studies[39-41] reported that the conversion of PrP^{C} to its misfolded PrP^{Sc} was mainly caused by the disruption in α-helices. To know the changes in α-helices brought out by mutation, we have computed phi (φ) and psi (ψ) angles of residues from α1-α3. Amino acids with backbone dihedral angles, φ= -67, ψ= -47 were considered to be in the α-helical region.[42] The φ and ψ angles of α1 residues as represented in Supp. Fig. 2 for the WT-PrP and its mutant calculated from the ensemble of trajectories (25000). In the WT-PrP, residue Asp^{144} showed sterically allowed angles, φ= -67 and ψ= -47 that corresponds to α-helix and also exhibited the backbone conformations to the bend region (φ= -150, ψ= -80) as observed in some of the trajectories (Fig. 2). Similarly, residues Tyr^{145}, Glu^{146}, Asp^{147}, Arg^{148}, Tyr^{149}, and Tyr^{150} were confined in ideal φ and ψ angles that correspond to α1. Furthermore, residues Arg^{151}, Glu^{152}, Asn^{153}, and Met^{154} displayed dihedral angles that correspond to both α-helix and turn region. In contrast to the WT-PrP, above mentioned residues in mutant, except Asn^{153} and Met^{154} showed rotationally well defined dihedral angles of α1. Further, residues Asn^{153} and Met^{154} were often

accounted in α1 in most of the trajectories thus increased the length of α1 by exhibiting their φ and ψ angle values which equivalent to α-helix. This result suggested that tiny changes in the φ and ψ angles of residues resulting in extend the length of α1 (Fig. 2B).

Further, φ and ψ angles of residues from α2 were computed and represented in Supp. Fig. 3 and 4 for the WT-PrP and its mutant respectively. It can be clearly seen that backbone conformation of residues from α2 in the WT-PrP displayed their desired φ and ψ angles to α-helix. While, the backbone dihedral angle of Gln^{172} from mutant was distributed in two clusters, the first and smallest cluster mainly linked to α-helix. The second and largest cluster of φ and ψ angles were mostly populated around -150 and 0 respectively resulting in the development of structurally disordered coil region as noticed after 8 ns simulation period (Fig. 2B). Furthermore, residues $Asn^{173\&174}$ involved in the formation of α-helix and also turn region due to change in the rotational freedom of backbone dihedral angles. Besides, residues Phe^{175}, Val^{176}, and His^{177} showed desired torsional angles correspond to α2 in most of the trajectories and also displayed an angle that linked to turn region. Again, residues Asp^{178} and Cys^{179} exhibited two conformations dependent clusters, the first and small cluster comprised of conformation that related to unstructured bend region by exhibiting φ= -150 and ψ= -60 to 100. The second and largest cluster contained the dihedral angles associated to α2 and turn segments. In addition, the backbone conformation of Val^{180} and Asn^{181} were mostly distributed around φ= -80 to -140 and ψ= 10 to 30, thereby involved in the formation diverse secondary structure. Again residues Ile^{182}, Thr^{183}, Ile^{184}, and Lys^{185} were displayed their favorable backbone torsional angles related to α-helix throughout the simulation period. At last, three terminal residues Gln^{186}, His^{187}, and Thr^{188} showed dihedral angles related to both α-helix and turn region. Similarly, the backbone dihedral angles of residues from α3 as depicted in Supp. Fig. 5 and 6 for WT-PrP and its mutant respectively. It can be clearly seen that residues from 202 to 224 in the WT-PrP showed their preferred φ and ψ angles linked to α3 during 50 ns simulation period, except Met^{206}, Glu^{207}, Arg^{208}, and Val^{209} were involved in the formation of turn region approximately from 12 to 42 ns simulation period. In contrast to the WT-PrP, φ and ψ angles of residues from α3 in mutant were mainly distributed in the region that corresponds to turn and 3_{10}-helix. Taken together, change in the backbone conformation of residues eventually cause distortion in the local folding of α2-α3, thus able to favour the transition of one secondary structure state into another in mutant V210I (Fig. 2B).

Conformational flexibility of mutant

How transition of one state secondary structure into another as noticed in mutant influencing its conformational dynamics can be portrayed by analyzing the backbone RMSD with respect to WT-PrP as represented in Fig. 4A as a function of time. Not surprisingly, it was found that mutant showed more backbone atomic deviation as observed within the ranges of 0.3-0.4 nm (average RMSD: 0.33 nm). It suggested the change in the conformational dynamics of mutant caused by the disruption in the local folding of α2-α3 (Fig. 2B). While, the WT-PrP displayed its typical conformational behavior linked with its stable secondary structural elements by exhibiting the backbone RMSD of 0.2-0.3 nm (average RMSD: 0.21 nm). In more detail, to know the observed changes in the conformational dynamics of mutant, we have further computed the average C_α atomic position of each residue in both WT-PrP and its mutant as represented in Fig. 4B. This result indicated that most of residues in mutant lost their preferred positions with respect to their C_α atom and also occurred between the ranges of 0.2 to 0.5 nm, implicating the more structural rearrangement. In particular, C_α atom of Asp^{144}, Tyr^{145}, and Glu^{146} from α1 exposed to molecular surface, in spite of their buried characteristic. Besides, two other charged residues Asp^{147} and Arg^{148} shifted towards the hydrophobic core of mutant. Moreover, C_α atoms of C-terminal residues Asp^{147}, Arg^{148} Tyr^{149}, Arg^{151}, Glu^{152}, and Asn^{153} from α1 also lost their preferred position and were rotated well into the hydrophobic core. In addition, C_α atom of β2-α2 loop residues Arg^{164}, Pro^{165}, Asp^{167}, Glu^{168}, Tyr^{169} and ser^{170} shifted towards the interior of mutant, where the C_α atom of residues Met^{166} and Asn^{171} were moved out significantly in comparison to residues in the WT-PrP. Moreover, C_α atom of residues His^{177}, Cys^{179}, and Lys^{185} from α2 (residues: 172-188) turned well towards the hydrophobic core of mutant and the other two residues Val^{176} and Val^{180} maintained their relative positions. Except, the above-stated residues, C_α atom of remaining residues from α2 were moved to the surface. Likewise, C_α atom of most of residues from α3 (residues: 202-224) were highly exposed to solvent, indicating the disturbance in the hydrophobic core of mutant.

It has been stated that protein function can be determined by the tertiary structure associated with its internal dynamics.[43] Thus, it is essential to emphasize the internal dynamics of mutant, because several MD simulations and NMR studies reported that backbone flexibility of PrP was linked to conformational conversion.[44] With this meaningful support, we have further

analyzed the internal dynamics of mutant by comparing with WT-PrP as a possible determinant for conformational conversion of PrP^{C} to PrP^{Sc}. To accomplish this, dihedral order parameter was used to measure the backbone flexibility28 as presented in Fig. 5A. This result demonstrated that residues Asp^{144}, Arg^{148}, Tyr^{150}, Arg^{151}, Glu^{152}, Asn^{153}, and Met^{154} from α1 in mutant exhibited slightly more rigidity, i.e., backbone conformation of these residues were distributed within the specified conformations. Where the other three residues Tyr^{145}, Glu^{146} and Asp^{147} from α1 showed higher S2 values, indicates increasing in backbone flexibility. Interestingly, the α2-α3 region in WT-PrP displayed rigid dynamics, exhibiting the S2 value of around 1. On the other hand, the α2-α3 region in mutant accounted fairly small S2 values implies increasing in internal dynamics which markedly played a sizeable role in the destabilization of α2-α3. Overall, increased dynamics of mutant suggested the structural instability may favor causing the conformational conversion.[44] Again, change in internal dynamics of mutant was further confirmed by PCA as depicted in Fig. 5B. Because, identifying the structural plasticity was especially beneficial for proteins involved in conformational diseases.[45] The height of the peaks represented in Fig. 5B indicated the magnitude of the residue flexibility with respect to C_{α} atom. Over again, this result was well correlated with the result obtained from dihedral order parameter. It can be seen that α1 region from mutant V210I showed slightly more rigidity along the first principle component in comparison to WT-PrP. Again, the β2-α2 loop and α2-α3 exhibited more conformational perturbation together with α2-α3 loop also displayed more frustration, important for the structural variation of CJD mutant.[45]

Misfolding of mutant revealed by Free energy landscape (FEL)

The ability of protein to fold its evolutionarily conserved structure is important for biological function. In recent years, understanding of protein folding was greatly improved by the development of Gibb's free energy landscape.[46-48] To reveal the misfolding of mutant associated with its energy, we have used coordinates that obtained through RMSD and Rg. The FEL plot of WT-PrP (A) and its mutant V210I (B) as depicted in Fig. 6, using the ensemble of reaction coordinates obtained from the largest cluster, which noticed between 20-40 ns simulation periods. The lowest energy conformations as represented in Fig. 6 signified by blue color, where the orange color described the meta-stable states. The WT-PrP displayed a well-defined global energy minima funnel-like basin and the basin that contained the lowest free

energy conformations were highly located at the RMSD = 0.26 nm and Rg of 1.42 nm (Fig. 6A). Whereas, the lowest energy conformations of mutant V210I were greatly found at the RMSD = 0.36 nm and Rg of 1.5 nm (Fig. 6B). This result suggested that misfolding of mutant eventually showed structurally more disorder, thereby exhibited the broadening of end-to-end distance of residues. Further, these lowest energy conformation clearly specified the stability of the structure, more often, it occurred in the funnel-like shape.[49] Collectively, the global energy minima of mutant was mainly comprised of decreasing in the content of α2-α3 and the conformational transitions within the basin were rapid.

Detailed structure analysis: PrP^{C} vs PrP^{Sc}

Further, we have performed a detailed structure analysis to get deeper insights into the structural disorder influenced by mutation V210I using the trajectory obtained at 30 ns, because this trajectory was identified as middle structure in the largest cluster. The comparison of WT-PrP (Fig. 7A) and its mutant (Fig. 7B) showed that they were superimposed with respect to the backbone atoms and showed the RMSD value of 7.6 Å. However, some local structural variations were observed in mutant, particularly in the α2-α3 region, β2-α2 loop, and at the interface of α2 and α3 which were good agreement with the experimental results.[20] Residue Val210 involved in the part of hydrophobic core and play an important role in providing stability to WT-PrP. Substitution of Ile instead of Val did not render major changes in hydrophobic interactions around the mutated site itself in comparison with WT-PrP. However, residue Ile^{210} provoked structural rearrangements of several other residues that were involved in hydrophobic interactions at the interface of α2-α3 (Fig. 7C). In the WT-PrP, residues Val^{180} and Val^{210} were positioned each other at the interface of α2 and α3 respectively and both the residues linked by direct hydrophobic interaction. Upon mutation, residue Val^{180} altered its side chain orientation significantly due to steric crowding. Moreover, substitution of Ile^{210} had the tendency to displace the side chains of Val^{176} and Ile^{184} when compared to their position in WT-PrP. Finally, these results confirmed the disruptions in various hydrophobic contacts that were usually present in WT-PrP. Further, these notable changes that were observed in mutant can be evaluated by the comparison of distance with respect to WT-PrP as illustrated in Table 1. It can be clearly seen that inter-residue Val^{180}-Ile^{184} and Val^{176}-Val^{180} distances were significantly longer in mutant by comparing with WT-PrP and these results were well correlated with experimental study.[20]

Residue Val^{176} in both WT-PrP and mutant do not exhibit a long-range interaction with the residue Tyr^{218}. Taken together, the mutual orientation of α2-α3 was altered significantly, and change in the helical twist was another outcome, substantially influenced the hydrophobic contacts within the globular domain.

Another region in mutant that displayed a noteworthy level of structural alteration was in the β2-α2 loop (Fig.7B). In the WT-PrP, β2-α2 loop had the tendency to develop a 3_{10}-helix (residues: 166 to 169), whereas the β2-α2 loop in mutant displayed a highly disordered coil and bend region. Again, in the WT-PrP, 3_{10}-helix stabilized by a hydrogen bond between the residues of Met^{166}O-Tyr^{169}H. In case of mutant, such a hydrogen bond was not observed; thereby β2-α2 loop in mutant exhibited diverse conformational dynamics. In addition, residue Tyr^{169} in WT-PrP positioned toward the interior of protein and formed π–π interactions with Phe^{175}, Tyr^{163}, Tyr^{162}, and, and Tyr^{218}. Upon mutation, the orientations of above-mentioned residues were altered remarkably; resulting in loss of those aromatic residues mediated π–π interactions. Particularly, the side chain of Tyr^{169} in mutant was varied greatly, thus displayed a highly solvent-exposed conformation. Besides, the orientations of Tyr^{163} and Tyr^{175} were also altered, as a consequence, the structural stability influenced by hydrophobic cluster as noticed in WT-PrP was absent in mutant. Collectively, the notable structural alterations as observed in the mutant was mainly manifested by the disturbance in long-range Tyr^{169}-Phe^{175}, Phe^{175}-Tyr^{218}, Tyr^{163}-Tyr^{218}, and Tyr^{163}-Phe^{175} distances as represented in Table 2 which were well correlated with experimental results.[20]

Further, we have aimed to add our knowledge on α-helices, because several studies reported that α2-α3 play a vital role in the conversion of PrP^{C} into PrP^{Sc}.[39-41] Principally, hydrophobic and hydrogen bonding interactions were likely involved in the protein stability and folding respectively. Misfolding of protein often turned out due to collapse in this forces.[50] Thus, to understand the distortion in the local folding of α-helices as noticed in mutant, we have computed the numbers of M-M hydrogen bonds that involved in the formation of α-helices. It can be seen in Table 3 that a total of six hydrogen bonds was noticed in α1 of WT-PrP, where, α1 in mutant had the propensity to form five hydrogen bonds. In comparison to WT-PrP, mutant had lost a hydrogen bond between the residues of Glu^{146}-Tyr^{150}, due to changes in the desired φ and ψ angles of those residues. It can be clearly seen in Fig. 7B that loss of M-M hydrogen bonds in

mutant showed biased disruption in the α2 and the complete distortion on α3. Accordingly, the α2 region in the WT-PrP comprised of twelve hydrogen bonds, while the 4-fold reduction was examined in the α2 region of mutant (Table 3). It could be due an unsatisfied position of backbone atoms of residues present in α2 of mutant, thus unable to form an essential hydrogen bonds that mainly involved in the formation of α2 in that specified time (30 ns). Particularly, backbone conformations of residues Gln^{172}, Asp^{178}, and Cys^{179} in mutant were not allocated in their preferred φ and ψ angles linked to α-helix. In comparison to the α2 region in mutant, local folding of α3 was completely distorted. Again, it could be due to the loss of M-M hydrogen bonds (Table 3) resulting in the development of 3_{10}-helix and turn region (Fig. 7B). All together, this results suggested that substitution of Ile at position 210 showed substantial effects on hydrophobic interactions at the interface of α2-α3 and local folding of α2-α3 as well, which may offer a possible conformational seed, required for the aggregation propensity of mutant PrP.

The combined effect of above stated interactions in mutant which presumably affects the overall folding. Furthermore, predicting the solvent-accessibility of α-helices which can assist in elucidating the folding of mutant. The accessible surface area of residues present in the α1-α3 of WT-PrP and its mutant as presented in Supp. Table 1. A total of 13 residues, seven residues were protruded out; especially the side chain of Tyr^{149} and Tyr^{150} was highly exposed to solvent as noticed in the α1 region of mutant. Where, the remaining six residues in mutant lost their desired position and were moved towards the hydrophobic core, despite their hydrophilic characteristic. Out of 17 residues as noticed in α2, 11 residues were rotated out to solvent, implicating highly solvent-accessible surface characteristic of α2 in mutant V210I. Likewise, most of residues in α3 also shifted towards the molecular surface when compared to the WT-PrP as represented in Supp. Table 1. Overall, this result confirmed the misfolding characteristic of mutant by exposing the hydrophobic residues to molecular surface. Again, it was important to describe the structural characteristic of β2-α2 loop, because several pathological mutations in the different part of PrP affect the conformation of the β2-α2 loop in a similar manner.[51] The structural rearrangement of the β2-α2 loop was mainly caused by changes in the orientation of Tyr^{169} as depicted in Fig. 8. In the WT-PrP, residue Tyr^{169} positioned in the interior of protein, in case of mutant, it was highly exposed to solvent, which may be considered as a marker of PrP^{C} to PrP^{Sc}. By comparing with WT-PrP, such a structural consequences as noticed in the mutant β2-α2 loop, eventually displayed the hydrophobic surface to solvent and this result seems to parallel features of partially

folded intermediate states of PrP^{Sc}.[52] Interestingly, residue Tyr^{169} identified as part of the epitope that was proposed earlier as a region that could enhance the binding of hypothetical facilitator of PrP^{Sc} conversion, known as "protein X" engaged in the development of TSE.[53,54] Therefore, the solvent exposed conformation of Tyr^{169} may enhance the propensity for inter molecular interactions of mutant with its yet unknown cellular PrP^{C} ligands. At last, in agreement with the NMR results, our MD results also revealed the possible role of mutation V210I on the flexibility of β2-α2 loop, local folding of α2-α3, and also the hydrophobic effect at the interface of α2-α3.

Conclusion

In summary, structural findings suggested that substitution of Ile on α3 influenced paramount disruptions in the local folding of α2-α3 and also have an effect in the hydrophobic interaction at the interface of α2-α3. Indeed, β2-α2 loop in mutant exhibited more structural perturbation resulting in increase the distance between this loop and α2. Besides, the altered conformational dynamics of β2-α2 loop mainly caused by the loss of 3_{10}-helix followed by the elimination of hydrophobic stacking interactions of Tyr^{169} with Phe^{175}, Tyr^{163}, Tyr^{162}, and Tyr^{218}. All together, the notable structural variations as noticed in the β2-α2 loop and on α2-α3 may promote the inter-molecular interactions of mutant with its yet un-known ligands. Finally, the detailed structure and dynamic properties of mutant V210I obtained in this study shed further light on the mechanism of conversion of PrP^{C} to PrP^{Sc}, might imply the novel approaches for effectual pharmacological intervention.

Acknowledgment

We thank the management of VIT University for providing facilities to carry out this work.

References

1. P. Chandrasekaran and R. Rajasekaran, Mol. Biosyst., 2016, 12, 850-859.

2. S. Giorgetti, A. Rossi, P. Mangione, S. Raimondi, S. Marini, M. Stoppini, A. Corazza, P. Viglino, G. Esposito, G. Cetta, G. Merlini ssand V. Bellotti, Protein Sci., 2005, 14, 696-702.

3. T. C. Bjorndahl, G. P. Zhou, X. Liu, R. Perez-Pineiro, V. Semenchenko, F. Saleem, S. Acharya, A. Bujold, C. A. Sobsey and D. S. Wishart, Biochemistry, 2011, 50, 1162-1173.

4. K. J. Knaus, M. Morillas, W. Swietnicki, M. Malone, W. K. Surewicz and V. C. Yee, Nat. Struct. Biol., 2001, 8, 770-774.

5. W. Chen, M. W. van der Kamp and V. Daggett, Biochemistry, 2010, 49, 9874-9881.

6. W. Chen, M. W. van der Kamp and V. Daggett, Biophys. J., 2014, 106, 1152-1163.

7. Y. Wen, J. Li, W. Yao, M. Xiong, J. Hong, Y. Peng, G. Xiao and D. Lin, J. Biol. Chem., 2010, 285, 31682-31693.

8. S. Lee, L. Antony, R. Hartmann, K. J. Knaus, K. Surewicz, W. K. Surewicz and V. C. Yee, EMBO J., 2010, 29, 251-262.

9. I. Biljan, G. Ilc, G. Giachin, J. Plavec and G. Legname, Biochemistry, 2012, 51, 7465-7474.

10. I. Biljan, G. Giachin, G. Ilc, I. Zhukov, J. Plavec and G. Legname, Biochem. J., 2012, 446, 243-251.

11. M. Meli, M. Gasset and G. Colombo, PLoS One, 2011, 6, e19093.

12. G. Ilc, G. Giachin, M. Jaremko, L. Jaremko, F. Benetti, J. Plavec, I. Zhukov and G. Legname, PLoS One, 2010, 5, e11715.

13. D. B. O'Sullivan, C. E. Jones, S. R. Abdelraheim, M. W. Brazier, H. Toms, D. R. Brown and J. H. Viles, Protein Sci, 2009, 18, 410-23.

14. G. Rossetti, X. Cong, R. Caliandro, G. Legname and P. Carloni, J. Mol. Biol., 2011, 411, 700-712.

15. R. I. Dima and D. Thirumalai, Biophys. J., 2002, 83, 1268-1280.

16. R. I. Dima and D. Thirumalai, Proc. Natl. Acad. Sci. U. S. A., 2004, 101, 15335-15340.

17. L. Calzolai and R. Zahn, J. Biol. Chem., 2003, 278, 35592-35406.

18. Y. Zhang, W. Swietnicki, M. G. Zagorski, W. K. Surewicz and F. D. Sönnichsen, J. Biol. Chem., 2000, 275, 33650-33654.

19. Q. Kong, J. L. Mills, B. Kundu, X. Li, L. Qing, K. Surewicz, I. Cali, S. Huang, M. Zheng, W. Swietnicki, F. D. Sönnichsen, P. Gambetti and W. K. Surewicz, Cell Rep., 2013, 4, 248-254.

20. I. Biljan, G. Ilc, G. Giachin, A. Raspadori, I. Zhukov, J. Plavec and G. Legname, J. Mol Biol., 2011, 412, 660-673.

21. H. J. C. Berendsen, D. Van der Spoel and R. Van Drunen, Comput. Phys. Commun., 1995, 91, 43-56.

22. H. J. C. Berendsen, L. Grigera and T. P. Straatsma, J. Phys. Chem., 1987, 91, 6269–6271.

23. M. Kaminski, G. A. Friesner, R. A. Tirado-Rives and L. W. Jorgensen, J. Phys. Chem. B, 2001, 105, 6474-6487.

24. N. Darden, T. York, and L. Pedersen, J. Chem. Phys., 1993, 98, 10089-10092.

25. O. Hess, B. Kutzner, D. Spoel and E. Lindahl, E, J. Chem. Theory Comput., 2008, 4, 435-447.

26. H. J. C. Berendsen, J. P. M. Postma, W. F. van Gunsteren, A. DiNola and J. R. Haak, J. Chem. Phy., 1984, 81, 3684-3691.

27. G. Vriend, J. Mol. Graph, 1990, 8, 52-56.

28. D. vander Spoel and H. J. C. Berendsen, Biophys. J., 1997, 72, 2032–2041.

29. G. Lipari and A. Szabo, J. Am. Chem. Soc., 1982, 104, 4546–4559

30. C. Kappel, U. Zachariae, N. Dölker and H. Grubmüller, Biophys. J., 2010, 99, 1596-1603.

31. S. Haider, G. N. Parkinson and S. Neidle, Biophys. J., 2008, 95, 296-311.

32. M. Laberge and T. Yonetani, Biophys. J., 2008, 94, 2737-2751.

33. P. Chandrasekaran and R. Rajasekaran, Mol. Biosyst., 2014 10, 1869-1880.

34. B. Han, Y. Liu, S. W. Ginzinger and D. S. Wishart, J. Biomol. NMR, 2011, 50, 43-57.

35. W. Kabsch and C. Sander, Biopolymers, 1983, 22, 2577-2637.

36. Z. Shi and N. R. Kallenbach, Proc. Natl. Acad. Sci. U. S. A., 2011, 108, 3-4.

37. K. M. Saravanan, H. Balasubramanian, S. Nallusamy and S. Samuel, Protein Eng. Des. Sel., 2010, 23, 911-918.

38. M. M. Gromiha and S. Selvaraj, Prog. Biophys. Mol. Biol., 2004, 86, 235-277

39. H. Wille, M. D. Michelitsch, V. Guenebaut, S. Supattapone, A. Serban, F. E. Cohen, D. A. Agard and S. B. Prusiner, Proc. Natl. Acad. Sci. U. S. A., 2002, 99, 3563-3568.

40. C. Govaerts, H. Wille, S. B. Prusiner and F. E. Cohen, Proc. Natl. Acad. Sci. U. S. A., 2004, 101, 8342-8347.

41. M. L. DeMarco and V. Daggett, Proc. Natl. Acad. Sci. U. S. A., 2004, 101, 2293-2298.

42. A. Q. Zhou, C. S. O'Hern and L. Regan, Biophys. J., 2012, 102, 2345-52.

43. R. Ishima and D. A. Torchia, Nat. Struct. Biol., 2000, 7, 740-743.

44. Y. Wen, J. Li, M. Xiong, Y. Peng, W. Yao, J. Hong and D. Lin, PLoS One, 2010, 5, e13273.

45. D. M. Gendoo and P. M. Harrison, PLoS Comput. Biol., 2012, 8, e1002646.

46. A. R. Dinner, A. Sali, L. J. Smith, C. M. Dobson and M. Karplus, Trends Biochem. Sci., 2000, 25, 331-339.

47. P. R. Batista, M. G. Costa, P. G. Pascutti, P. M. Bisch and W. de Souza, Phys. Chem. Chem. Phys., 2011, 13, 13709-13720.

48. Y. Miao, S. E. Nichols and J. A. McCammon, Phys. Chem. Chem. Phys., 2014, 16, 6398-6406.

49. V. Lesch, A. Heuer, V. A. Tatsis, C. Holm and J. Smiatek, Phys. Chem. Chem. Phys., 2015, 17, 26049-26053.

50. G. Haran, Curr. Opin. Struct. Biol., 2012, 22, 14-20.

51. B. Christen, F. F. Damberger, D. R. Pérez, S. Hornemann and K. Wüthrich, Proc. Natl. Acad. Sci. U. S. A., 2013, 110, 8549-8554.

52. A. C. Apetri, K. Surewicz and W. K. Surewicz, J. Biol. Chem., 2004, 279, 18008-18014.

53. G. C. Telling, M. Scott, J. Mastrianni, R. Gabizon, M. Torchia, F. E. Cohen, S. J. DeArmond and S. B. Prusiner, Cell, 1995, 83, 79-90.

54. K. Kaneko, L. Zulianello, M. Scott, C. M. Cooper, A. C. Wallace, T. L. James, F. E. Cohen and S. B. Prusiner, Proc. Natl. Acad. Sci. U. S. A., 1997, 94, 10069-10074.

Table 1 Intra- and inter-helical distance between the residues from α2 and α3

	V180($C^{\gamma 1}$)-I184($C^{\delta 1}$)	**V176($C^{\gamma 1}$)-V180($C^{\gamma 2}$)**	**V176($C^{\gamma 1}$)-Y218($C^{\varepsilon 1}$)**
WT-PrP	4.2 Å	3.7 Å	9.2 Å
V210I	8.5 Å	7.8 Å	10.9 Å

Table 2 Distance between the residues involved in the interface of β2, α2, and α3

	Y169(C^{ζ})-F175(C^{ζ})	**F175(C^{ζ})-Y218($C^{\varepsilon 1}$)**	**Y163($C^{\varepsilon 2}$)-Y218($C^{\delta 1}$)**	**Y163($C^{\varepsilon 2}$)-F175(C^{ζ})**
WT-PrP	7.1 Å	5.4 Å	8.9 Å	4.3 Å
V210I	9.13 Å	9.5 Å	11.4 Å	13.3 Å

Table 3 Number of hydrogen bonds involved in α1-α3

	WT-PrP	V210I
α1	143 Ser O-H Asp 147	143 Ser O-H Asp 147
	144 Asp O-H Arg 148	144 Asp O-H Arg 148
	145 Tyr O-H Tyr 149	145 Tyr O-H Tyr 149
	146 Glu O-H Tyr 150	147 Asp O-H Arg 151
	147 Asp O-H Arg 151	148 Arg O-H Glu 152
	148 Arg O-H Glu 152	
α2	172 Gln O-H Val 176	181 Asn O-H Lys 185
	173 Asn O-H His 177	182 Ile O-H Gln 186
	175 Phe O-H Cys 179	183 Thr O-H His 187
	176 Val O-H Val 180	
	177 His O-H Asn 181	
	178 Asp O-H Ile 182	
	179 Cys O-H The 183	
	180 Val O-H Ile 184	
	181 Asn O-H Lys 185	
	182 Ile O-H Gln 186	
	183 Thr O-H His 187	
	184 Ile O-H Thr 188	
α3	199 Thr O-H Val 203	
	200 Glu O-H Lys 204	
	210 val O-H Cys 214	
	211 Glu O-H Ile 215	
	212 Gln O-H Thr 216	
	213 Met O-H Gln 217	
	214 Cys O-H Tyr 218	
	216 Thr O-H Arg 220	
	217 Gln O-H Glu 221	
	218 Tyr O-H Ser 222	

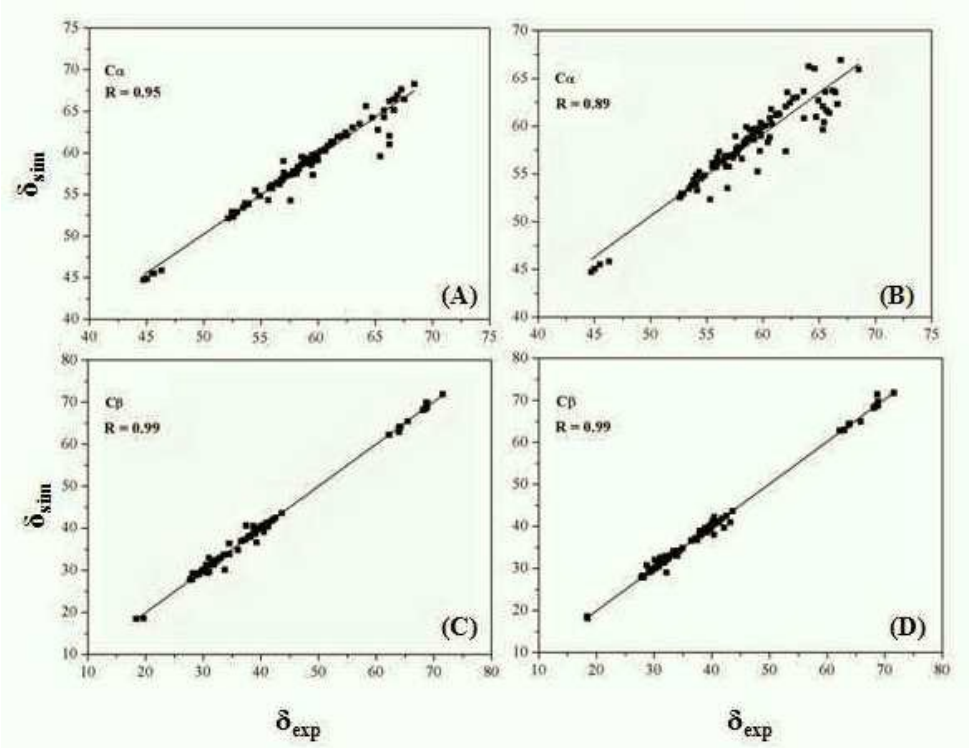

Fig. 1 Correlation of experimental and simulation chemical shifts. The Pearson correlation coefficient (r) was mentioned at the top left of each panel. Left panels indicated the C_α **(A)** and C_β **(C)** chemical shift value of WT-PrP. Right panels showed the C_α **(B)** and C_β **(D)** chemical shift value of mutant V210I.

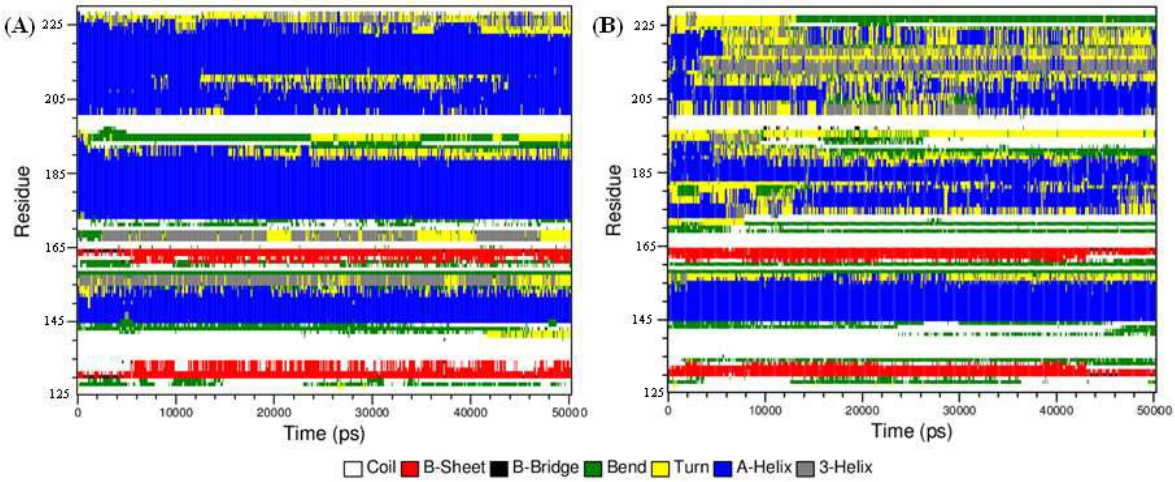

Fig. 2 Time evolution of secondary structure profile of WT-PrP **(A)** and its mutant **(B)** as a function of time.

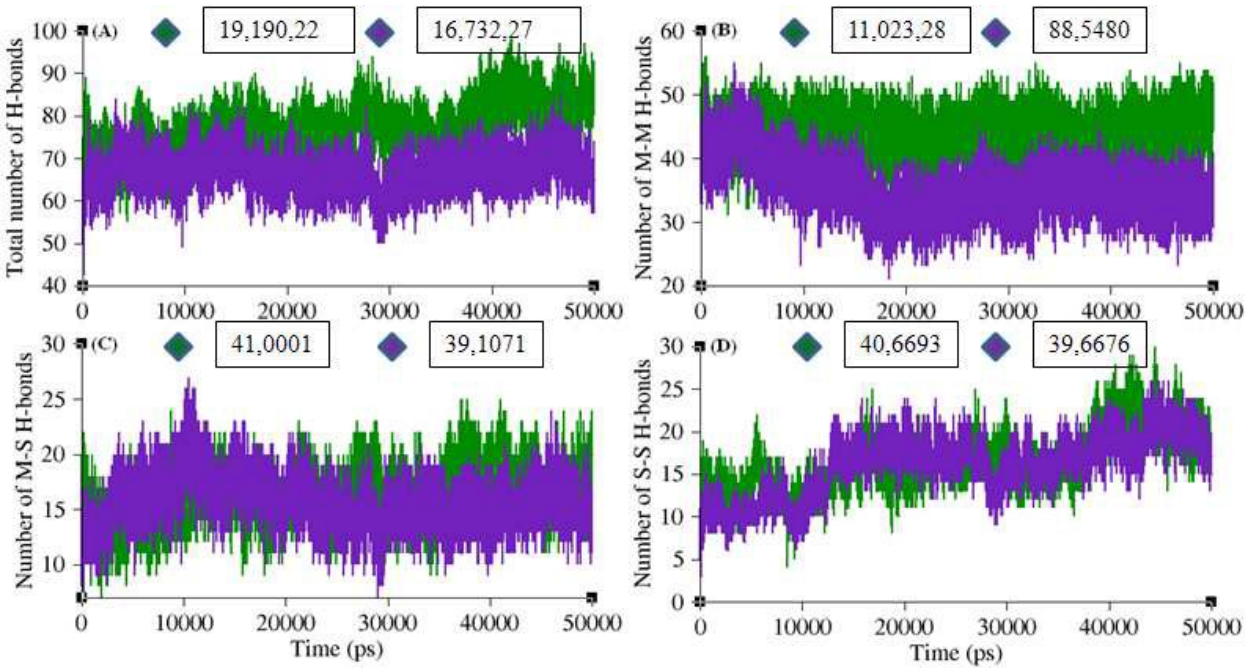

Fig. 3 Hydrogen bonding interactions observed in the WT-PrP (green) and its mutant (indigo) as a function of time. **(A)** Total number of H-bonds. **(B)** M-M H-bonds. **(C)** M-S H-bonds. **(D)** S-S H-bonds. Number of H-bonds was mentioned in box.

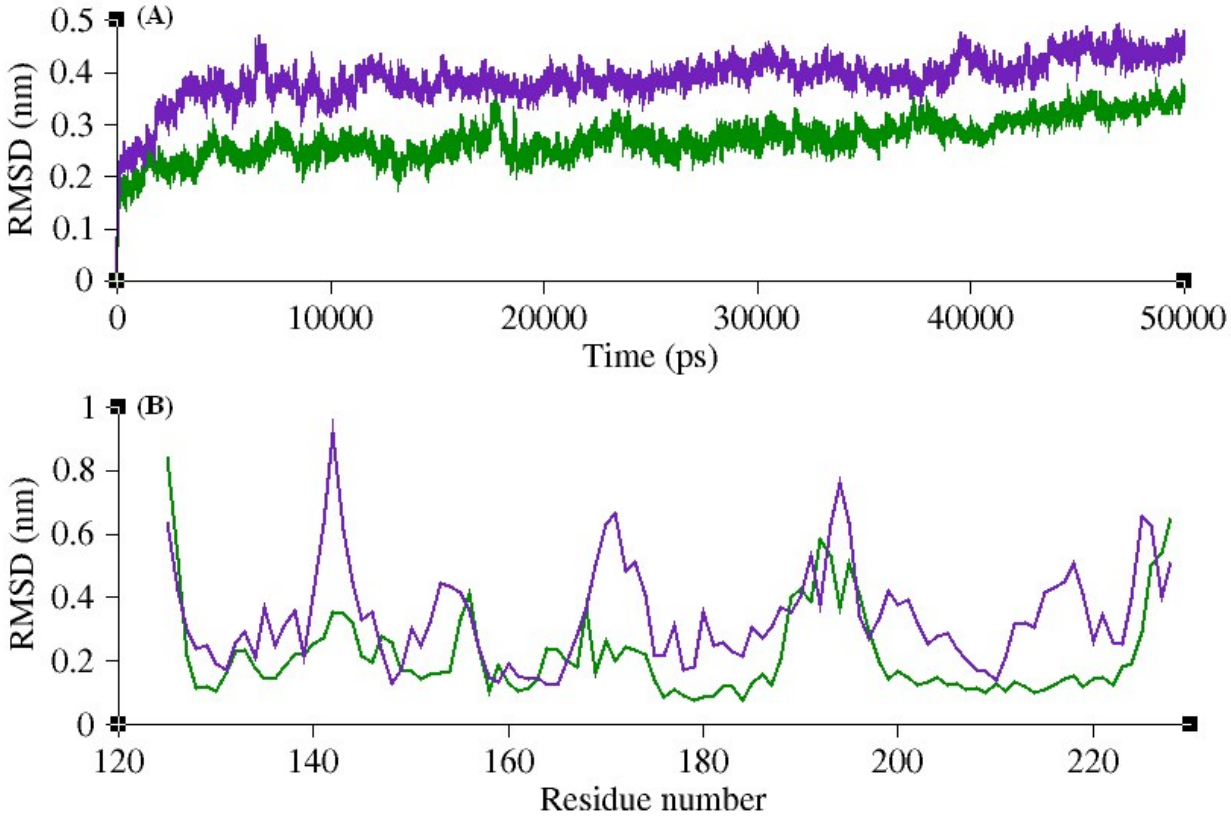

Fig. 4 (A) Backbone RMSD of WT-PrP (green) and its mutant (indigo). (**B)** Average C_α RMSD of residues present in the WT-PrP (green) and its mutant (indigo).

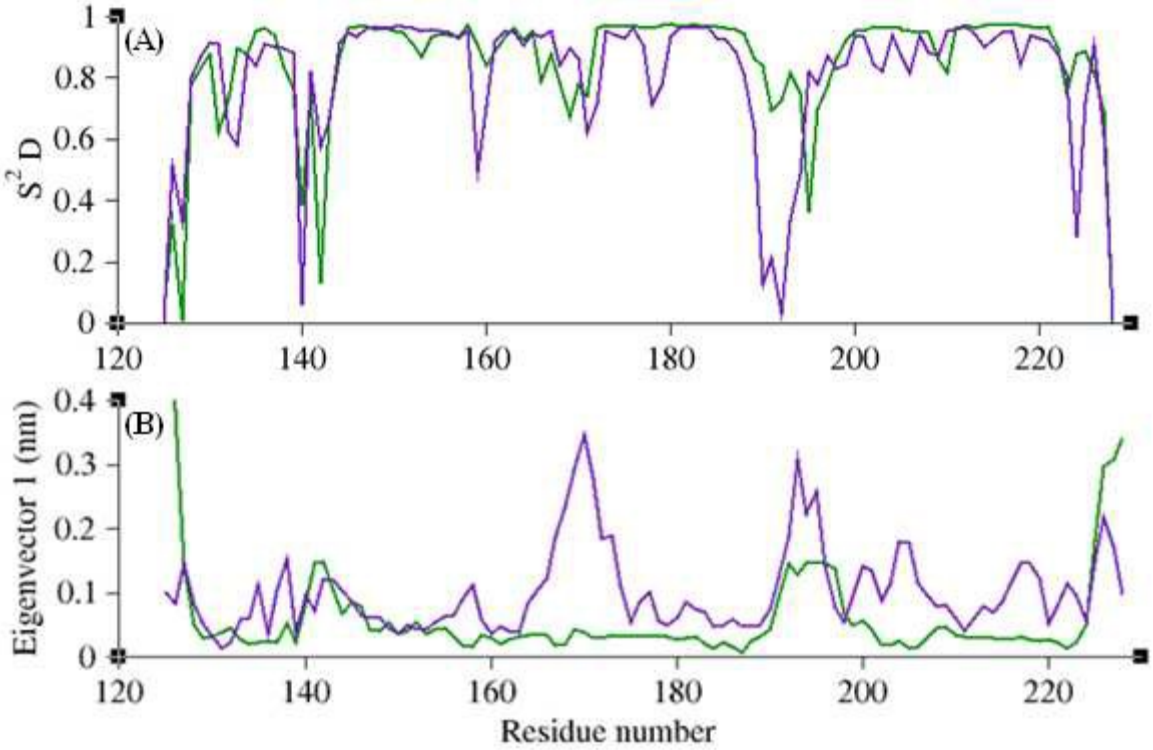

Fig. 5 (A) Internal dynamics of WT-PrP (green) and its mutant (indigo). Values near 1 indicated rigid backbone and low values represent the increased backbone flexibility. (**B**) The residue displacement of WT-PrP and its mutant along the first principle eigenvector.

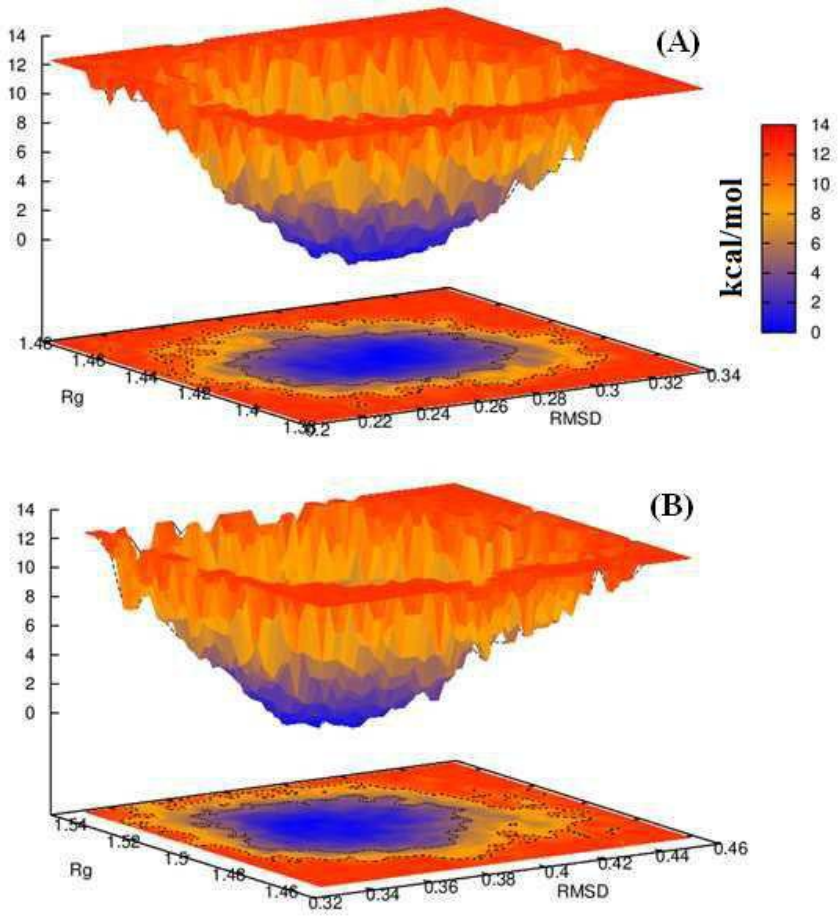

Fig. 6 FEL to the WT-PrP (**A**) and its mutant (**B**): RMSD vs Rg.

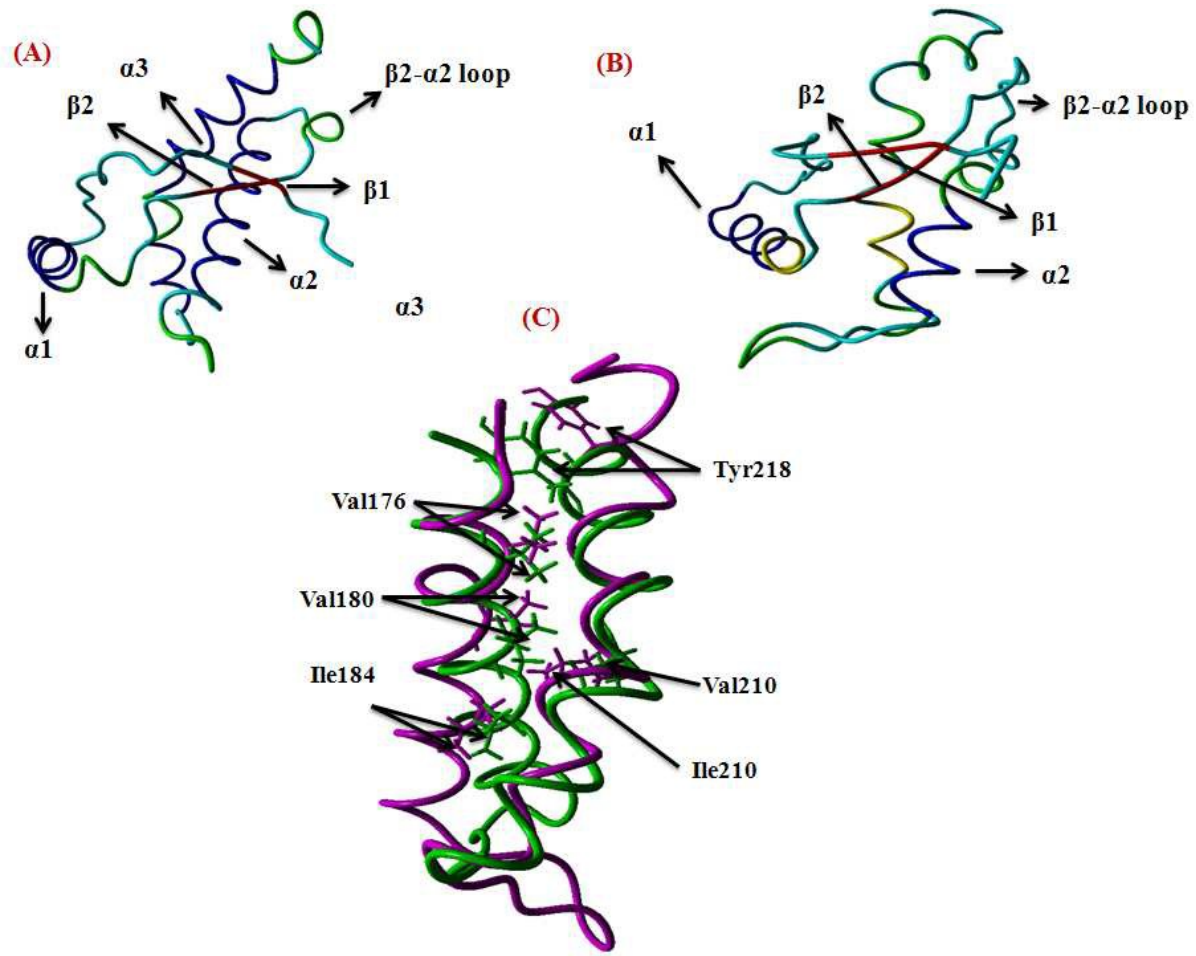

Fig. 7 Secondary structural elements present in the WT-PrP (**A**) and its mutant (**B**) during 30 ns simulation period. (**C**) Hydrophobic interactions observed between α2 and α3 of WT-PrP (green) and its mutant (indigo). Residues were represented as stick model.

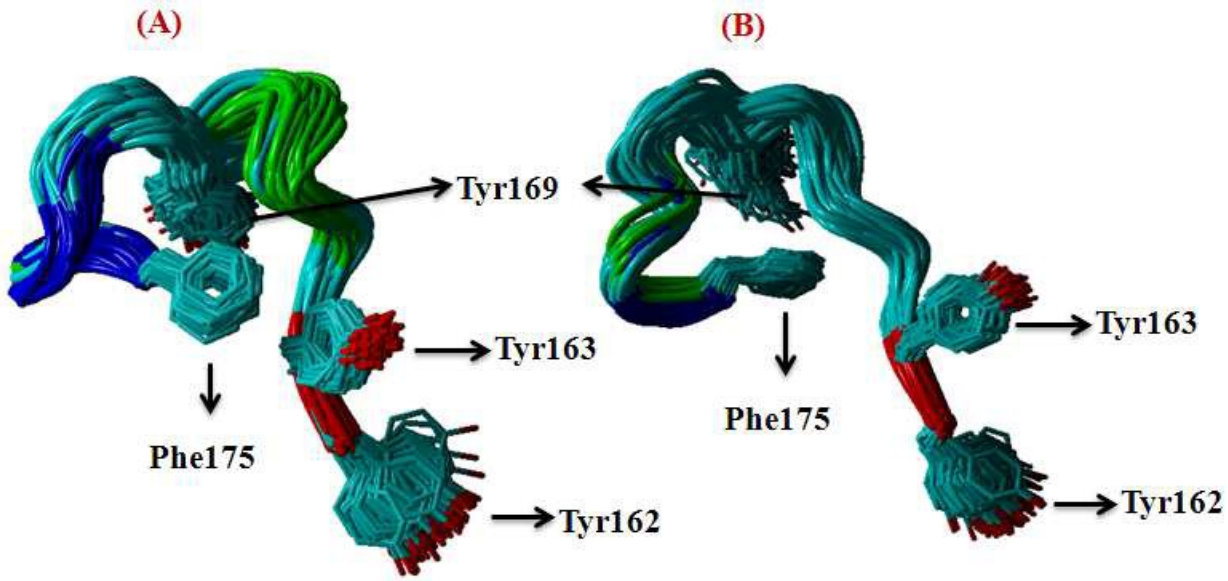

Fig. 8 Structural details of β2-α2 loop present in the WT-PrP (**A**) and its mutant V210I (**B**).